Phaseless Spherical Near-Field Antenna Measurements With Reduced Samplings

Nicolas Mézières, Laurent Le Coq, Benjamin Fuchs

Phaseless Spherical Near-Field Antenna Measurements with Reduced Samplings

Nicolas Mézières, Laurent Le Coq, and Benjamin Fuchs *Senior Member, IEEE*

***Abstract*—The ever-growing complexity of radiating systems asks for always more challenging radiation pattern characterizations requiring time consuming field acquisitions and high-cost facilities. Consequently phaseless, or magnitude-only, measurements have recently regained of interest as they prevent the tedious and difficult task of phase acquisition. Consequently, it allows the use of cheaper or more versatile measurement setups like drone measurements or easier high-frequency measurements. However, the difficulty is shifted to the notoriously difficult resolution of the phase retrieval problem, which instability is commonly mitigated by the acquisition of a large number of phaseless field samples. A procedure enabling a reliable and accurate phaseless antenna measurement from a reduced number of spherical NF samples based on the two scan technique is proposed. Its efficiency and stability, that relies on the systematic determination of a good starting point, is validated by representative simulations and experimental cases performed on various antenna structures.**

***Index Terms*—Antenna measurements, near field, phaseless measurement, phase retrieval, phase estimation, wave functions.**

I. Introduction

The characterization of radiation pattern of antennas is ubiquitous nowadays and the design of complex radiating systems calls for high-cost equipment and specific expertise. Consequently, a huge effort has been and is still done in the development of measurement techniques and dedicated algorithms to mitigate the numerous errors and difficulties inherent to the pre- and post-processing of antenna measurements. Two main lines of studies have been followed. On the one hand, the reduction of the number of (complex) field samples required to perform an accurate antenna measurement has been addressed by many works as it directly impacts the field acquisition time. Smaller measurement samplings can be achieved by harnessing sparse recovery of Spherical Wave (SW) expansion [1], [2] and the optimization of the sampling distribution [3]. The geometry of the Antenna Under Test (AUT) can also be exploited by analytical [4] or numerical [5], [6] means to provide a tailored basis for radiated field expansion. A numerical basis can also be constructed by an appropriate set of simulations [7]. Despite the reduction of the number of measurement samples, the need to accurately acquire the complex field remains, calling for costly measurement setups and possibly long calibration steps, especially when going up in frequency. On the other hand, the development of phaseless measurement aims at reducing the constraints on the antenna characterization setup itself by avoiding the tedious and sensitive acquisition of the phase.

An overview of some magnitude-only measurement procedures can be found in [8]. The considered phaseless procedure uses the scans of two concentric NF spheres and the field is expanded on Spherical Waves (SW) [9]. The two independent sampling surfaces provide the magnitude differences essential to the appropriate reconstruction of the phase. To perform well, most phaseless antenna characterization approaches require at least twice the number of samples used in standard complex field measurement procedure (according to the so-called Nyquist sampling rates), as half of the information (i.e. the phase) is missing. In other words, oversampling is often necessary to achieve a reasonable accuracy with phaseless measurements. Indeed, having more data is known to be highly beneficial for the convergence of Phase Retrieval (PR) algorithms [10]. A detailed overview of sampling sizes found in the literature for phaseless measurement is provided in Section II-C. Furthermore, the SW possess a common pattern: they are ordered with respect to how fast they oscillate (spatially). This known SW structure is leveraged to build a weighted regularization scheme that helps the resolution of the phaseless antenna characterization problem from a reduced number of field samples.

This paper proposes a phaseless spherical antenna characterization approach from a small number of Near-Field (NF) samples using the two scan method, combining thereby both features: the phaseless measurements and the reduction of the number of field samples. It is organized as follows. The SW expansion of electromagnetic fields and the phaseless formulation of antenna characterization are given in Section II. A review on the sample sizes commonly used in phaseless is also provided in this section. The proposed method to reduce the sampling sizes for phase retrieval is motivated and described in Section III. An extended study on a canonical horn antenna is led in Section IV. The phaseless procedure is tested and validated on measurement data in Section V and conclusions are drawn in Section VI.

II. Phaseless Spherical Measurement

A. Spherical Wave Expansion

The electric field $\mathbf{E}$ radiated by the AUT can be expanded using the SW as

$$\mathbf{E}(r,\theta,\varphi) = \frac{k}{\sqrt{\eta}} \sum_{smn} Q_{smn} \mathbf{F}_{smn}(r,\theta,\varphi) \tag{1}$$

N. Mézières and L. Le Coq are with the Institut d'Électronique et des Technologies du numéRique (IETR), Université de Rennes 1, Rennes, France e-mail: laurent.le-coq@univ-rennes.fr.

B. Fuchs is with the Federal Office of Communications, Biel, Switzerland
Manuscript received x, 2023; revised x, 2023.

with k the wavenumber, η the admittance of the propagation medium and (r, θ, φ) the spherical coordinates [9]. The functions $\mathbf{F}_{smn}$ are the SW and Q_{smn} the spherical coefficients to be retrieved. The indices n and m are the degree and the order of the SW, respectively. Finally, s denotes the propagation mode. In practice, the series in (1) is often truncated to $n \leq N = \lfloor ka \rfloor + 10$ with a the radius of the minimum sphere (the sphere of smallest radius enclosing the sources and centered at the origin of the coordinate system) and $\lfloor \cdot \rfloor$ the floor function. The number of measurements given by the Nyquist sampling rate on the full sphere is $M = 2(2N+1)(N+1)$ and the number of complex unknowns is $U = 2N(N+2)$, $(M \approx 2U)$.

Given a sampling of the radiated field, the expansion (1) is rewritten as the following linear system of equations

$$\mathbf{y} = \mathbf{A}\mathbf{x} \tag{2}$$

where $\mathbf{y}$ gathers the measurement data, $\mathbf{A}$ is the matrix containing the SW at the sampling positions and $\mathbf{x}$ contains the spherical coefficients Q_{smn}. In NF, the SW expansion (1) and consequently the matrix $\mathbf{A}$ can be adapted according to the transmission formula [9], [11] to account for the radiation pattern of the probe.

B. Phaseless Spherical Measurements with Two Scans

In phaseless measurements, the system (2) leading to the characterization of the antenna becomes

$$|\mathbf{y}| = |\mathbf{A}\mathbf{x}| \tag{3}$$

since only the magnitude of the field is available. The problem (3) is solved in the least-square sense for complex $\mathbf{x}$

$$\min_{\mathbf{x}} \left\| |\mathbf{A}\mathbf{x}| - |\mathbf{y}| \right\|^2. \tag{4}$$

where $\| \cdot \|$ denotes the Euclidean norm or 2-norm and the absolute value is applied element-wise. Its resolution implies special care on the sampling strategy and specific algorithms that allow for the retrieval of the complex SW expansion coefficients in $\mathbf{x}$. To mitigate the ambiguities arising when solving (4), an efficient and well known approach is the two scan technique [8]. Each scan is performed on surfaces that might share or not the same geometry to provide the magnitude differences that are necessary to determine a phase. In the proposed spherical phaseless NF procedure, the two scans are performed on two concentric spheres. Thus the matrix $\mathbf{A}$ contains two SW matrices $\mathbf{A}_1$ and $\mathbf{A}_2$ for each measurement sphere S_1 and S_2, respectively.

C. Size of Phaseless Samplings

This section details the sizes of the samplings that can be found in the literature regarding phaseless antenna measurements. The quantity M denotes the number of measurements corresponding to the Nyquist sampling rate for complex samples in planar, cylindrical or spherical configurations. The sampling sizes are also evaluated by the sampling ratio $\Delta = \frac{M}{U}$. In a standard spherical complex measurement, the Nyquist sampling rate gives $\Delta \approx 2$. If two scans with equal sampling sizes are performed, the sampling ratio per scan is denoted δ and $\Delta = 2\delta$. A summary of the sampling sizes that can be found in cited works is given in Table I. The asterisk symbol * after the number of samples denotes that the reported sampling size concerns an electrically small antenna, of diameter smaller than 2λ.

For the phaseless procedures using two planes, a pioneer work based on plane wave projections has been performed in [12] from $2M$ samples (two acquisition planes with the classical sampling step $\lambda/2$), later followed by a refined version in [13] using the same sampling sizes. A more generic approach based on plane waves and Gerchberg-Saxton (GS) algorithm with $4M$ samples to characterize the field using spiral samplings (twice the regular, complex, sampling rate on each plane) was successfully done in [14]. A first equivalent current approach can be found in [15] for Far-Field (FF) characterization or diagnostic with $2.8M$ samples. Finally, using equivalent currents and the Reweighted Amplitude Flow (RAF) required $3.1M$ and $4M$ in [16] for improved results. A cylindrical procedure using a single surface but with an interferometry method based on two probes is proposed in [17] and is validated with $2M$ samples.

An extended study on a two concentric spherical acquisitions for phaseless can be found in [11] using the GS algorithm and where the number of sampling points is equal to $4M$ (thus the sampling ratios for the total sampling and for each scan are respectively $\Delta \approx 8$ and $\delta = 4$). A similar work in [18], using the Wirtinger Flow algorithm [19], used $3M$ for a given antenna with the same field acquisition technique. The involved phase ambiguities are investigated in [20] and a number of $1.25M$ is reached by using the PhaseLift algorithm [21] but for an electrically small antenna (diameter less than 2 wavelengths λ) with centered beam, which are known to be easier to characterize as observed in [11]. A number of $1.5M$ is also achieved in [22] from similar configuration and also with an electrically small antenna. Finally, $2M$ and above (up to $5M$) measurements are used in [23] while studying the sampling distributions and geometries of the second measurement surface. The various parametric studies on the two spheres provided in [24] use between $2M$ and $3M$ samples. Sparse recovery for phaseless was used in [25]. Some results for sample sizes close to $1.25M$ are shown for small dipole arrays (around 1.5λ in diameter) and only a few significant coefficients on the kept SW band (10% of non-zero coefficients) but $2M$ at least are said to be required to guarantee accurate PR. Finally, partial phaseless measurements on a single spherical surface and interferometry have been performed in [26] and indicated that at least $2M$ samples were necessary to obtain successful reconstructions but that $2.5M$ and $3M$ provided significantly more stable results.

As a conclusion, current studies rely on significant oversamplings to perform phase retrieval. In general, sampling sizes of at least $2M$, twice the standard complex sampling rates, are used. Most papers note or demonstrate that accuracy is improved significantly by the acquisition of more field samples (using more scans or more dense distributions). Lower sizes, close to the standard complex measurement ones, can be found for simulation examples with electrically small antennas only (diameter $< 2\lambda$).

TABLE I
CLASSICAL SAMPLING SIZES FOR PHASELESS MEASUREMENT

Ref.	Method	Sampling Size
Planar measurements		
[12]	Plane Wave projections	$2M$
[13]	Plane Wave projections	$2M$
[14]	GS and spiral samplings	$4M$
[15]	Equivalent currents	$2.8M$
[16]	Equivalent currents and RAF	$3.1M$
[17]	Interferometry (+ Cylinder)	$2M$
Spherical measurements		
[11]	GS	$4M$
[18]	Wirtinger Flow	$3M$
[20]	Phaselift	$1.3M$*
[22]	Phaselift	$1.5M$*
[23]	Wirtinger Flow (Sphere + other)	$2M$
[24]	Various convex PR	$2M$
[25]	Sparse recovery	$2M$ ($1.25M$*)
[26]	Interferometry	$2M$
This work	Regularization and RAF	M

(* = AUT diameter $< 2\lambda$)

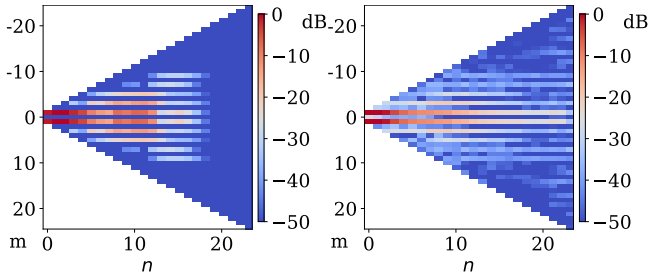

(a) Reference (b) Aliased spectrum

Fig. 1. Simulated horn antenna: (a) reference SW expansion coefficients for $s = 1$ (TE modes) and (b) an instance of improperly retrieved version because of under-sampled phaseless measurements.

III. REGULARIZATION FOR REDUCED SAMPLINGS

A. Motivation

1) Reduced samplings and Aliasing: Phaseless problems are notorious for their ill-conditioning and solution uniqueness problems. Improper sampling strategies, measurement surface setups, or bad tuning of post-processing approaches are all sources of potential errors in the obtained characterization. In the context of SW expansion, the size of the samplings is one of the most important error source, as thoroughly investigated in [11]. The impact of too coarsely sampled data on the retrieved SW expansion coefficients is shown in Fig. 1 for a horn antenna at 10 GHz of minimum sphere $a = 7\,\mathrm{cm}$. It leads to aliasing which is observed as a spread of the significant SW coefficients across all degrees n. High-degree SW present faster oscillations since the degree n determines simultaneously the maximal number of (spatial) oscillations over θ and φ (as the order m satisfies $|m| \leq n$). They allow for a better fitting of the sampled data but might prevent the proper convergence of PR procedures by generating local minima or convergence traps.

2) Spherical Wave Representation: The characterization of the radiated field of antennas from phaseless measurements

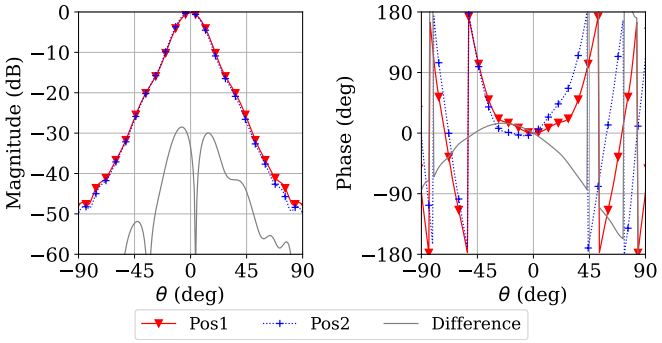

Fig. 2. Simulated horn antenna: radiated NF co-polarization on the H-plane, (*left*) magnitude and (*right*) phase, at 45 cm for two coordinate system origins distant from $1.2\,\mathrm{cm} \approx 0.4\lambda$.

relies on the magnitude differences occurring between the NF spheres S_1 and S_2. A small change of the AUT position impacts the spectral representation because of the difference in phase pattern. Conversely, the magnitude is not modified significantly until sufficiently large shifts are performed. Therefore, the SW expansion, and thus the phase, cannot be uniquely determined for magnitudes differences that are below the dynamic range of the measurement configuration. This is illustrated by the NF emitted for the simulated horn antenna for two different positions distant of $1.2\,\mathrm{cm} \approx 0.4\lambda$ at a NF distance of $45\,\mathrm{cm}$ in Fig. 2. The shift of the antenna induces small changes in amplitude, which is the only information available, but modifies significantly the phase pattern.

3) Penalty on High-Degree SW: A main source of error in phaseless comes from the aliasing that mostly happens in the high-degree part of the spectrum. A first available method is to filter out the high-degree contributions after a first PR algorithm run. Then, this filtered solution can be fed to a new run of the algorithm with a finely tuned starting phase. This solution has been evoked in [27] and is more extensively studied in [28], from which the implementation is taken to provide the benchmarks. Another way is to impose a constraint on these functions with faster variations so they are only introduced at a cost. This cost is implemented in this paper as a weight used within a regularization procedure. As for the filters, the regularization significance can be adjusted between different consecutive runs to progressively reach more refined solutions and to avoid inappropriate constraints on the mode distribution.

B. Optimisation Problem Formulation

1) General Form: A weighting matrix $\mathbf{W}$ is introduced to promote the low-degree SW for the reasons given in the previous section. The proposed regularized PR problem is

$$\min_{\mathbf{x}} \left\| |\mathbf{A}\mathbf{x}| - |\mathbf{y}| \right\|^2 + \mu^2 \left\| \mathbf{W}\mathbf{x} \right\|^2 \tag{5}$$

where μ is the regularization coefficient, or regularizer. The matrix $\mathbf{W}$ is diagonal and the weight $W_{n,n}$ associated to $\mathbf{F}_{smn}$ is $W_{n,n} := 2n + 1$, the number of SW having degree n for a given propagation mode s. Other choices of weights could be made but this simple one turns out to be efficient: it takes into account that more and more functions are available to fit

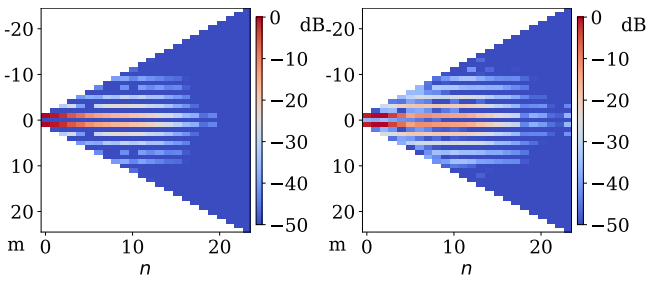

(a) $\mu = 0.5$ (b) $\mu = 0.1$

Fig. 3. Simulated horn antenna: SW expansion coefficients retrieved from under-sampled phaseless NF data with a single run of RAF algorithm for two values of regularizer μ.

the data as the degree increases while avoiding overly strong constraints on the power distribution. This new problem is a sum of two squared terms, and share similarities with the well-known Tikhonov problem/ridge regression. The minimization of the first term, the data-fitting term, is equivalent to (4). The second one introduces the proposed regularization. Such formulation was first introduced in [29] for phaseless FF magnitude measurement and interpolation.

2) Resolution Details: The regularization term added between problems (4) and (5) can be dealt with using standard routines by setting the following equivalent formulation (see Appendix A)

$$\min_{\mathbf{x}} \left\| |\mathbf{A}_W \mathbf{x}| - |\mathbf{m}| \right\|^2 \tag{6}$$

where $\mathbf{A}_W = \begin{bmatrix} \mathbf{A} \\ \mu \mathbf{W} \end{bmatrix}$ and $|\mathbf{m}| = \begin{vmatrix} \mathbf{y} \\ \mathbf{0} \end{vmatrix}$. The proposed regularized problem is therefore transformed back into a standard phaseless problem with more equations. The matrices $\mathbf{A}$, $\mathbf{W}$ and the measurement vector $\mathbf{y}$ should be normalized (relatively to their sum of squares) for PR algorithm stability and to keep similar values for μ between the different cases. Resolution of (6) is achieved using the RAF algorithm from PhasePack [30] according to benchmarks provided in [16], [24]. The impact of the regularization term on the retrieved complex SW expansion coefficients is shown in Fig. 3 for the same simulation of the horn antenna. As expected, a larger regularizer μ induces a shrinking of the coefficients toward lower degrees n.

C. Phase Initialization

Phase initialization is a great deal in phaseless problems as it heavily conditions the final results. In this paper, it is proposed to perform a first resolution of the regularized phaseless problem (5) with a purposely large regularizer μ_1 in order to find a coarse solution with low-degree SWs. This over-regularized solution, while not accurate, provides a good starting phase that is tailored to the measurement problem. Thus, it is used to derive a phase initialization for a second resolution with a smaller μ_2. The determination of the values μ_1, μ_2 are discussed in Section IV-C. The whole procedure can be summed up as

1) Resolution of (6) using RAF with spectral initialization and a large regularizer μ_1.
2) Computation of a new starting phase from over-regularized solution.
3) Resolution of (6) using RAF with the so-determined starting phase and a fine tuned μ_2.

Since the first run is for initialization purposes only and the regularizer μ_1 is large, only a few iterations are necessary as the convergence is fast. The interest of the proposed two step regularization instead of one is justified in Section IV-B and the claimed fast convergence of the first step is illustrated in Section IV-D4.

D. Reconstruction Metric and Methodology

The success of the phaseless characterization is evaluated by comparing the retrieved FF in $\widetilde{\mathbf{y}}_{FF}$ from the phaseless NF to the reference one, $\mathbf{y}_{FF}$. This comparison is achieved point-wise by the error signal defined as follows

$$\text{Error}(\mathbf{y}_{FF}, \widetilde{\mathbf{y}}_{FF}) = \frac{||\mathbf{y}_{FF}| - |\widetilde{\mathbf{y}}_{FF}||}{\max_i |\mathbf{y}_{FF,i}|}. \tag{7}$$

The mean of this error signal is the Equivalent Noise Level (ENL) and both are given in dB. The error signals displayed in the 2D maps of the total field magnitude are the norm of the error signals computed from both components independently. The comparison of the FF magnitudes provides a single, straightforward, indicator of a coherent retrieved phase in NF as faithful FF reconstruction is not possible otherwise, especially when changing the description of the polarization from E_θ, E_φ to Ludwig-3 for example. All NF samplings distributions follow the *igloo* sampling strategy [31] as it is close to be uniform on the sphere and thus avoid spatial redundancy, which is important matter in PR [22], [24]. The same angular samplings are used for both NF spheres. The FF distance is evaluated using the Rayleigh definition, i.e. $\frac{2(2a)^2}{\lambda}$. The sampling sizes are evaluated using the sampling ratio δ for one scan or the total sampling ratio Δ, where $\Delta = 2\delta$ as angular samplings are the same on both spheres.

IV. Numerical Validations and Benchmark

Numerical investigations are first led on the simulation of a horn antenna in order to discuss the conditions for efficient and reliable use of the proposed technique. In particular, the settings of the approach (choice of the regularizers) and its performances with respect to competing techniques are addressed, demonstrating its efficiency and reliability.

A. Simulated Horn Antenna: Configuration

This antenna is modelled after the one pictured Fig. 11 and simulated using CST [32] at 10 GHz. It has a minimum sphere of radius $a = 7\,\text{cm}$ hence a SW truncation order of $N = 24$. The FF data are exported on a dense full sphere sampling in order to provide a reference SW expansion coefficient set. These coefficients are used to generate data on NF spheres at distances of 20 and 30 % of the FF. Unless stated otherwise, the PR algorithm (RAF) runs are of 100 and 900 iterations with regularizers μ_1 and μ_2, respectively (for all presented cases), and the sampling ratio is $\delta = 1.06$ (for this section only).

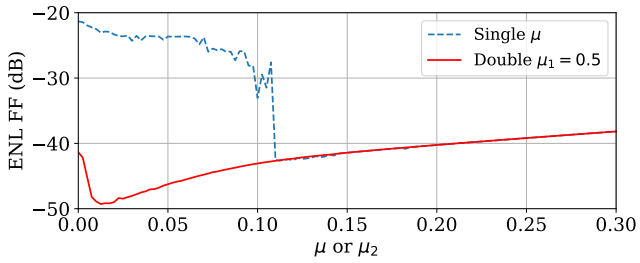

Fig. 4. Simulated horn antenna: comparison of FF reconstruction accuracy from the regularized phaseless problem using a single regularizer or double regularization steps with $\mu_1 = 0.5$.

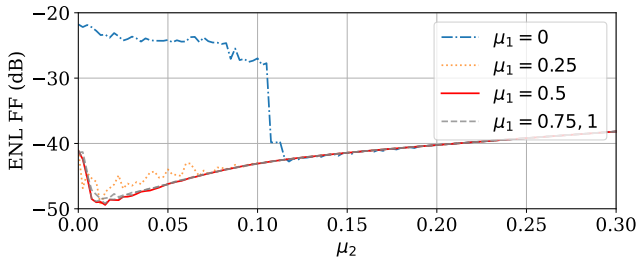

(a) Choice of the first regularizer μ_1

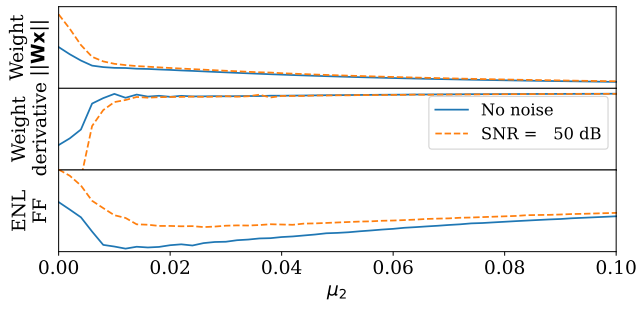

(b) Choice of the second regularizer μ_2 ($\mu_1 = 0.5$)

Fig. 5. Simulated horn antenna: impact of the choices of regularizer for both runs, μ_1 and μ_2, on the FF reconstruction.

B. Single and Double Regularization

The method solves the regularized phaseless problem (6) twice where the regularizer μ is first set to μ_1 and to μ_2 for a second run. The first resolution with large μ_1 enables to find a good initial solution and the second one with the smaller μ_2 to determine an accurate solution. The choice and tuning of the regularizer values are discussed in the next section. The comparison between a double regularization and a single run of 1000 iterations (i.e. same number in total) with only one regularizer μ is shown in Fig. 4. It is clear that the double regularization approach allows for more accurate reconstructions, also emphasizing on the importance of the phase initialization in PR.

C. Tuning of the Regularizers

The accuracy of the FF reconstruction relatively to both μ_1 or/and μ_2 is illustrated in Fig. 5. The FF reconstruction accuracy in ENL for various choices of μ_1 are compared in Fig. 5.a. As shown, the choice of this value is not critical as soon as it is sufficiently large, thanks to the normalization of the matrices in (6). This value has been set to $\mu_1 = 0.5$ for all presented cases. Looking at Fig. 5.b, we understand how the value of μ_2 can be chosen from observing the variation of the weight, the optimal value being located at the corner of the weight curve of the solution according to $\mathbf{W}$, a well known criterion in many regularization contexts [33], [34]. This corner can be identified by computing the derivative of the weight relatively to μ_2 (by finite differences). It also turns out that all presented cases yield the same kind of curves for both regularizers. Indeed, the first regularizer μ_1 gives a relevant initialization for a second, more refined, computation. The second regularizer performs a trade-off between the fitting to the data and the significance of the penalty induced by the weighting matrix. A value of $\mu_2 \approx 0.02$ is close to optimal in all presented cases and investigated sampling ratios δ and is consequently used throughout the whole paper for convenience.

D. Proposed Regularization vs Other Methods

The reconstruction performances of the proposed regularization approach are compared to other methods as a function of the sampling ratio δ. The tested methods and used acronyms are reported in Table II.

1) Configuration: The phaseless data are generated from the reference SW coefficients on two spheres S_1 and S_2 located at 20 and 30 % of the FF distance and two PR procedures are used for comparison; the RAF and the GS algorithms. The maximal total iteration number is set to 2000 in this section to make sure the convergence is reached for all algorithms to avoid unfair comparisons. For completeness, combination with filtering strategies are also compared as they have been shown to increase stability and accuracy [28]. The filters are either based on maximum modulus, the nm-MT (for Maximum Thresholding, all coefficients below a threshold in magnitude are set to 0) or low pass filter n-LPF (for Low-Pass Filter, all coefficients above a given degree N are set to 0). When using RAF, only the n-LPF one is used with the following settings; the coefficients are put to 0 above $N = 10$ and $N = 20$ at one and two thirds of the total number of iterations respectively (iterations number 666 and 1322 here). When using GS, implementation and parameters are set according to [28] and are not detailed further in this work. The regularizer values, when used, are set to $\mu_1 = 0.5$ and $\mu_2 = 0.02$. The GS runs are started with the phase of a dipole, as done in [11] for example. This configuration is tested on the simulation data without and with an added white noise of SNR 50 dB.

2) Sampling Ratio and Simulation Data (no noise): The results are reported in Fig. 6.a. The two step regularization procedure provides stable and accurate results for all samplings with $\delta \geq 1$. Smaller ratios, $\delta \leq 1$, also provide good ENLs in this case. The comparison with GS runs is given in the lower graphic. The proposed procedure outperforms the other tested approaches for low sampling ratios with steady accuracy

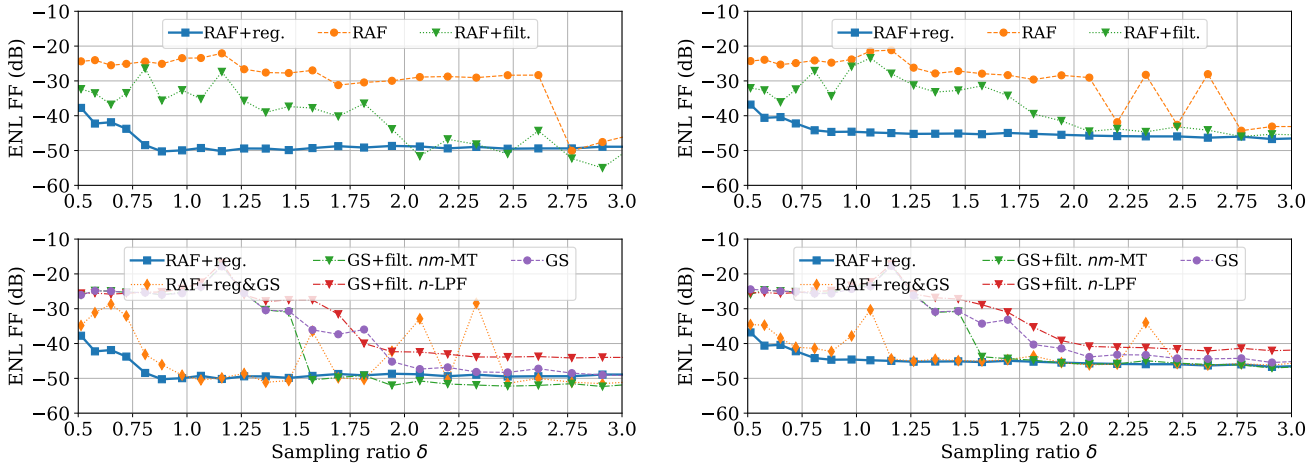

(a) Simulation data.

(b) Simulation data with additive noise, SNR = 50 dB.

Fig. 6. Simulated horn antenna, reconstructed FF accuracy for different sampling ratios δ: (*up*) comparison of RAF with regularization (reg.), filters (filt.) or nothing, (*down*) GS runs with and without filters (nm-MT or n-LPF) with phase initialization coming from a dipole or the over-regularized RAF solution with $\mu = 0.5$.

results. When the sampling sizes are large enough, the GS results are slightly more accurate as the second regularizer μ_2 is fixed to 0.02 for all samplings, which is non-optimal in that case. Indeed the best values of μ_2 are smaller for large samplings, as regularization is less necessary.

TABLE II
SUMMARY OF BENCHMARKED METHODS

Method	Description
GS	Standard Gerchberg-Saxton
GS+filt. n-LPF	GS with periodical low-pass filter
GS+filt. nm-MT	GS with periodical maximum based filter
RAF	Standard Reweighted Amplitude Flow
RAF+reg.	RAF with two step regularization
RAF+filt.	RAF with periodical low-pass filter
RAF+reg&GS	RAF with regularization to initialize GS

3) Sampling Ratio and Simulation Data with Noise: The results are reported in Fig. 6.b. In this case as well, the use of the two regularization steps with RAF allows for stable and accurate recovery for all sampling ratios from $\delta \geq 1$. There is no longer improvements by using GS for large sampling ratios as regularization now also helps at reducing the impact of noise. In terms of number of NF samples, it means that using more than $0.8U = 0.8 \times 2N(N+2) \approx 1000$ samples per NF phaseless scan does not lead to significantly more accurate results, whereas $2.1U \approx 2600$ samples at least are required without regularization and $1.6U \approx 2000$ samples when using the GS algorithm with filters.

4) Measurement Error and Convergence Speed: The measurement error is the relative error between the found reconstruction and the measurement data, defined by $\| |\mathbf{Ax}| - |\mathbf{y}| \| / \|\mathbf{y}\|$ in Phasepack [30]. It indicates how accurate is the resolution of (4) for each iteration of the algorithm. This error is reported for the RAF runs with filter, regularization or no processing in Fig. 7 for the standard sized sampling ratios $\delta = 2.07, \Delta = 4.14$, so that all methods converge

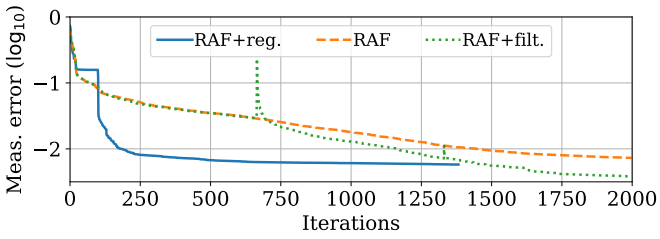

Fig. 7. Simulated horn antenna: measurement error during the RAF runs for the case $\delta = 2.07$, same notations as in Fig. 6.

appropriately. The two step regularization converges much faster to the algorithm tolerance (around 1300 iterations). Note that the smallest measurement error reached at the last iteration is slightly above in this case compared to the RAF run with filters (RAF+filt.) as it also includes the regularization term $\|\mathbf{Wx}\|$ in its computation, i.e. the measurement error is $\| |\mathbf{A}_W\mathbf{x}| - |\mathbf{m}| \| / \|\mathbf{m}\|$. Indeed, as reported in Fig. 6, for $\delta = 2.07$, the accuracy of the retrieved FF (quantified here by the ENL) are similar for both approaches. The change of regularizer between μ_1 and μ_2 at the 100th iteration is seen as a drop at this point. The flat curve before that point shows that the first step is achieved in just a few iterations. The application of the filters are visible as spikes at iterations 666 and 1322.

5) Summary: The approach exhibits the following features, as observed in the case of the investigated horn antenna:

- It allows for accurate results from a sampling ratio $\delta \geq 1$ per NF sphere (instead of $\delta \geq 2$ as classically done).
- It provides stable accuracy levels and is resilient to noise.
- No significant or no improvements at all are observed by the use of other methods for large sampling sizes.
- It speeds up the convergence of the PR algorithm.

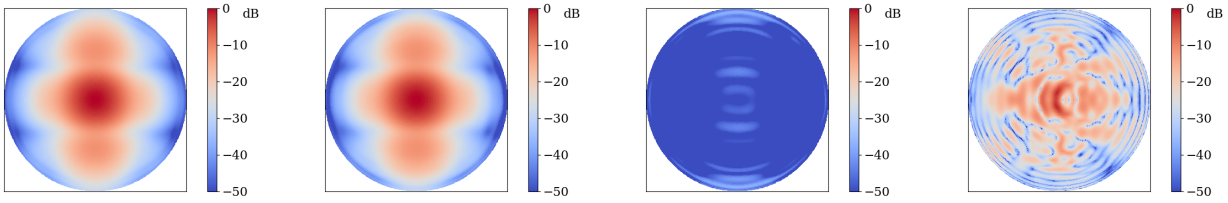

(a) Reference (b) From regularization (RAF+reg.) (c) Error (reference vs RAF+reg.) (d) Error (reference vs GS+filt.)

Fig. 8. Simulated horn antenna with $\delta = 1.06$: (a,b) total electric FF magnitude, (c) error with respect to the reference pattern and (d) error when using the GS algorithm with filters from the same sample.

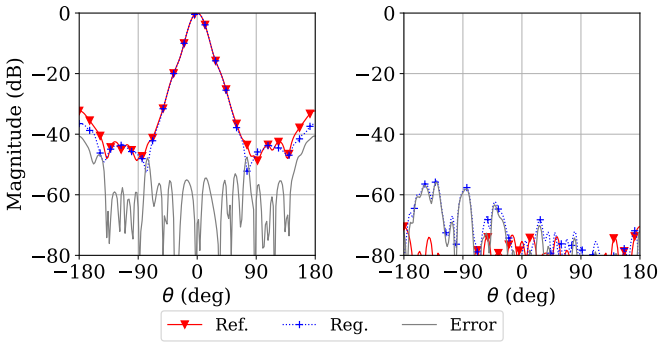

Fig. 9. Simulated horn antenna: reconstructions of the FF (*left*) co and (*right*) cross-polarizations in the H-plane from the NF data ($\delta = 1.06$).

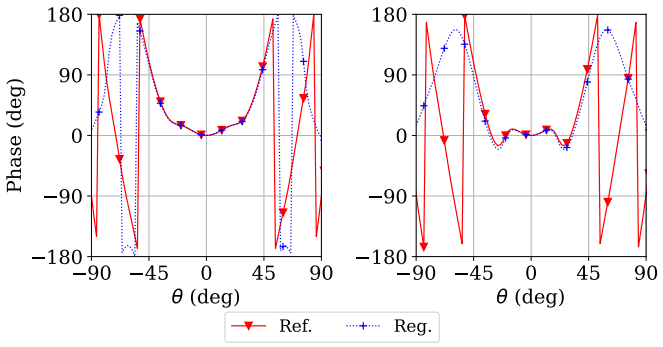

Fig. 10. Simulated horn antenna: FF co-polarization reconstruction of the phase in the (*left*) H-plane and (*right*) E-plane ($\delta = 1.06$). A constant phase shift has been added so that both curves pass through $0°$ at $\theta = 0°$.

E. Reconstruction Results

The 2D reconstructions of the simulated horn antenna FF for the case of a sampling ratio $\delta = 1.06$ per scan are reported in Fig. 8 and a cut in the H-plane is given in Fig. 9 for magnitude and in both planes for the co-polarization phase in Fig. 10. The results are quite accurate despite the reduced sampling sizes ($\approx 1.1M$ in comparison to a standard complex measurement). One can observe significant phase differences occurring outside of the main beam which are inherent to the non-uniqueness problems mentioned in Section III-A. The 2D reconstruction in Fig. 8 also shows the error signal when filters are used instead of regularization (tuned as described in the benchmark in Section IV-D), further illustrating the limitation of a simple thresholding approach for such reduced samplings.

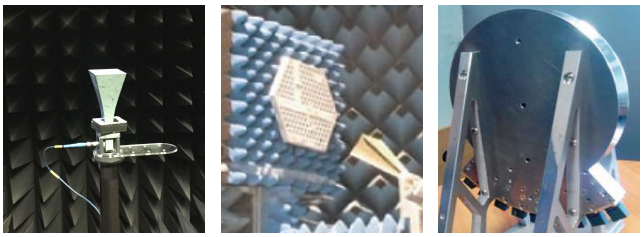

(a) Horn (b) Reflectarray (c) Lens

Fig. 11. Pictures of the measured antennas: (a) horn at 10 GHz in the MVG Starlab, (b) the reflectarray and (c) the Luneberg lens both measured at 12 GHz in the former CACENDRA anechoic chamber at IETR.

V. Validations on Experimental Data

Validations are lead on data coming from measurements. A summary of the obtained results in ENL between a dense reference and reconstructions obtained from the GS and the RAF algorithm are provided in Table III for samplings with classical size in phaseless ($2M$, $\delta = 2$) with reduced ones (M, $\delta = 1$). The GS algorithm is also used with the nm-MT filter implemented as in [28] for completeness.

A. Horn Antenna

The horn antenna, in Fig. 11.a, has been measured at 10 GHz in the MVG Starlab [35]. The so-derived complex spherical coefficients are used to generate the phaseless NF data. The considered minimum sphere has a radius of $a = 9\,\mathrm{cm}$ hence a SW truncation order of $N = 28$ (it differs from the simulation as the antenna is not centered in the Starlab). The two NF spheres are located at 20 and 30 % of the FF distance. 1700 field samples are considered per scan, which corresponds to a sampling ratio $\delta = 1.01$. The reconstructions of both polarization magnitudes in FF in the E and H planes are shown in Fig. 12. The ENL between the reconstructed FF and the reference one is $-42.5\,\mathrm{dB}$. The reconstruction accuracy is satisfactory despite the small sampling size.

B. Reflectarray

The experimental data comes from the measurement of the reflectarray displayed in Fig. 11.b. The system has been measured at 12 GHz at IETR in the FF. The resulting complex spherical coefficients are used to generate the phaseless NF data. The considered minimum sphere has a radius of $a = 16\,\mathrm{cm}$ hence a SW truncation order of $N = 50$. The two NF spheres are located at 10 and 15 % of the FF distance. There

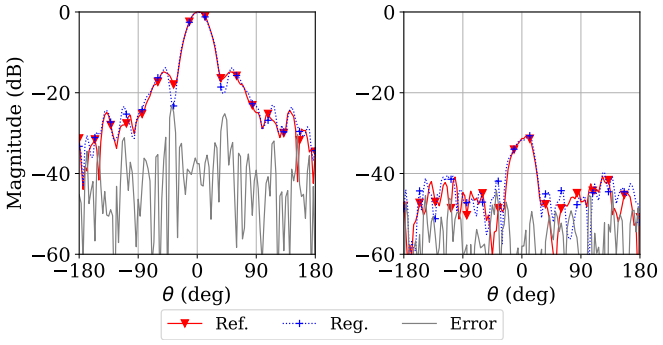

(a) E-plane

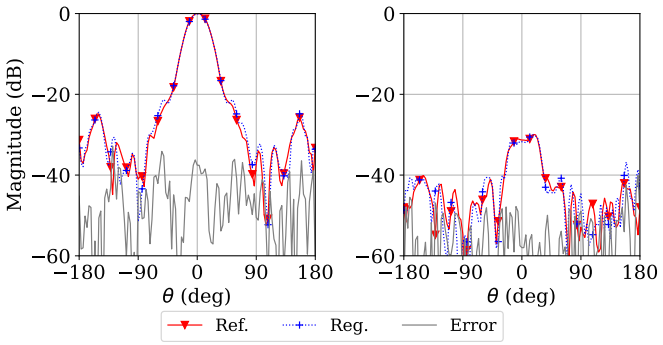

(b) H-plane

Fig. 12. Measured horn antenna: reconstructions of the FF (*left*) co- and (*right*) cross-polarizations in E and H planes from the NF data ($\delta = 1.01$).

were 5310 data per scan, corresponding to a sampling ratio $\delta = 1.02$. The 2D reconstructions of the field magnitude in the FF are shown in Fig. 13 and both polarization magnitudes in the main cutting plane in Fig. 14. Reconstructions show a good agreement despite the small phaseless sample. When using the GS algorithm with or without the filter, sampling ratios δ of 2.3 and 2.5 per NF scan, or equivalently sampling sizes of $\approx$ 12000 and 13000 respectively, are required for the same accuracy level. They are much larger than the 5310 samples used with the regularization approach.

C. Luneburg Lens Antenna

The measurement of the lens antenna in Fig. 11.c has been performed at 12 GHz at IETR in the FF. The parameters (minimum sphere, NF sampling distributions) are the same as in the case of the reflectarray. The 2D reconstructions of the field magnitude in the FF are shown in Fig. 15 and both polarization magnitudes in the main cutting plane in Fig. 16. A fairly good overall reconstruction is achieved but the reconstruction errors are not negligible as shown in Fig. 15.c. This observation can be explained by the more significant presence of radiated power in high degrees in the SW expansion of the field. However, the 2D errors made from using twice the number of samples ($\delta = 2.01$) is also reported and the ENL value can be found in the Table III. It shows that much larger samplings (10450 instead of 5310 points) do not lead to a much better accuracy, as already seen in Section IV-D.

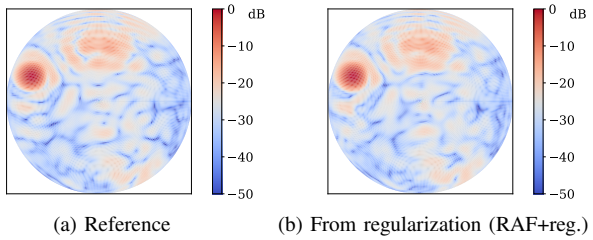

(a) Reference (b) From regularization (RAF+reg.)

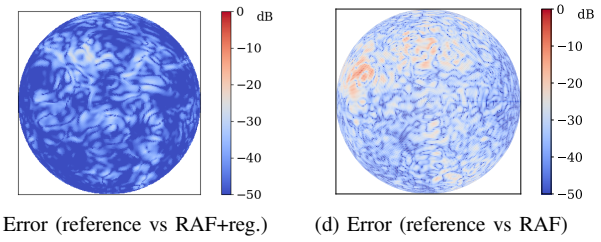

(c) Error (reference vs RAF+reg.) (d) Error (reference vs RAF)

Fig. 13. Measured reflectarray with $\delta = 1.02$: (a,b) total electric FF magnitude, (c) error with respect to the reference pattern and (d) error when using the RAF algorithm without regularization.

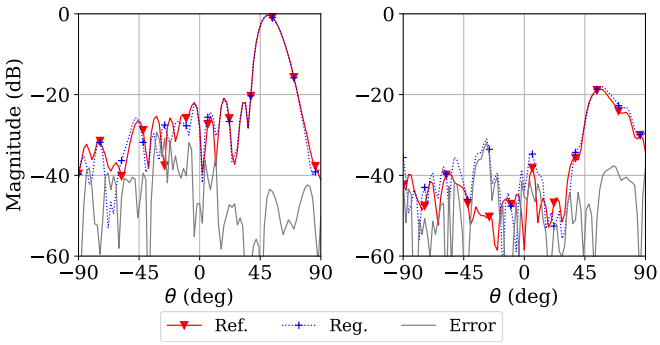

Fig. 14. Measured reflectarray: reconstructions of the FF (*left*) co- and (*right*) cross-polarizations in the principal plane from the NF data ($\delta = 1.02$).

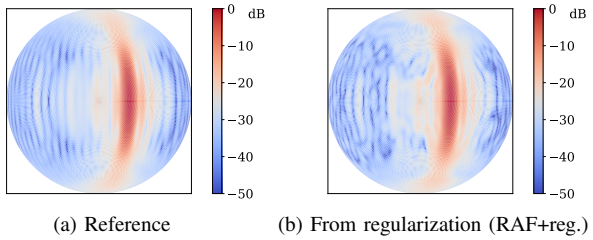

(a) Reference (b) From regularization (RAF+reg.)

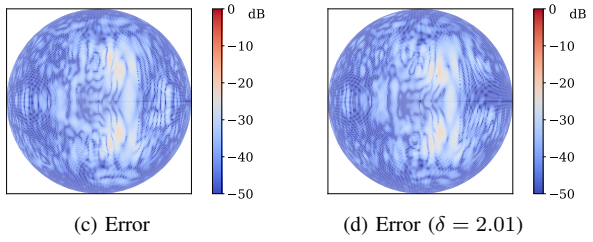

(c) Error (d) Error ($\delta = 2.01$)

Fig. 15. Measured lens antenna with $\delta = 1.02$: (a,b) total electric FF magnitude, (c) error with respect to the reference pattern and (d) error when using a twice larger field sample, $\delta = 2.01$.

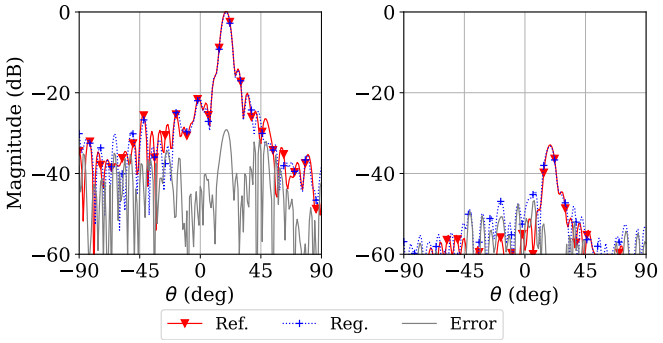

Fig. 16. Measured lens antenna: reconstructions of the FF (*left*) co- and (*right*) cross-polarizations in the principal plane from the NF data ($\delta = 1.02$).

TABLE III
EXPERIMENTAL VALIDATIONS: FAR-FIELD RECONSTRUCTION ACCURACY IN ENL

Antenna	Size	GS	GS+filt.	RAF	RAF+reg.
	Standard Phaseless Sampling Size ($\approx 2M$)				
Horn	6912	-43.3	-44.2	-23.2	-43.5
Reflectarray	20900	-36.8	-38.6	-37.6	-42.8
Lens	20900	-38.1	-41.8	-36.9	-40.7
	Reduced Sampling Size ($\approx M$)				
Horn	3400	-26.4	-26.2	-21.4	-42.5
Reflectarray	10620	-35.5	-33.8	-35.4	-41.1
Lens	10620	-35.8	-36.0	-31.1	-40.2

D. Summary

As reported in Table III, all the FF radiation patterns are reconstructed at an accuracy of at least $-40\,\mathrm{dB}$ in mean using NF phaseless data with sampling ratio $\delta \approx 1$ per sphere (total one of $\Delta \approx 2$) using the proposed approach (RAF+reg.). Such sampling ratio corresponds to having M measurements, the number advocated by the Nyquist sampling rate in a complex measurement. With the stop-and-go measurement configuration and a mechanical polarization change done in the IETR anechoic chambers with an *igloo* sampling strategy, the reflectarray and lens antenna both require 6h50 (3h18 for moving, 3h32 for frequency sweep and data recover) for each scan instead of 12h25 (5h49 for moving, 6h36 for frequency sweep and data recover) if a standard number of phaseless field samples of $2M$ is used. For the same configuration but with a continuous acquisition of the *igloo* sampling (sweep in φ, cut in θ, only a few measured frequencies and data registered for each cut), the measurement times are of 1h40 for M measurements and 2h30 for $2M$ measurements. In this case, the measurement duration is nearly proportional to the number of performed cuts. In the meantime, the field reconstruction mean error is only slightly improved of $1.7\,\mathrm{dB}$ in the worst presented case with the larger field samples. Table III also shows that the accuracy is much more steady and that the field samples were not large enough even with the classical number of phaseless field samples in the reflectarray case for the other methods to achieve the same accuracy level. Let us remind that the presented results might be improved, as the value μ_2 is fixed to 0.02 instead of being fine tuned. It has to be noted that both the reflectarray and the Luneburg lens antenna have tilted main beams, which are known to be more difficult for phaseless procedures, as observed in [11], as the SW expansion coefficients inevitably spread significantly over the order m. It is worth pointing out that the proposed approach is robust with respect to the number of samples as soon as $\delta \geq 1$ per scan. This robustness comes both from the systematic choice of a good initial solution and the way that the final solution is chosen thanks to the proposed regularized approach.

VI. CONCLUSION

A procedure to efficiently reduce the sampling sizes in phaseless antenna spherical measurements on two concentric spheres has been proposed and validated both numerically and experimentally on medium sized antennas up to around 12 wavelength in diameter. The method relies on a regularization approach composed of 2 steps. The first step provides an over-regularized solution used as a tailored phase initialization for the second step, namely the accurate resolution of the phaseless antenna characterization problem. The total number of phaseless field samples is reduced to roughly the same as standard complex spherical measurements, which means half of the commonly advised number of phaseless samples in the literature. The proposed regularization approach is applicable straightforwardly to other spherical phaseless configurations, including different field sampling schemes and with readily available routines.

APPENDIX A
EQUIVALENCE OF OPTIMIZATION PROBLEMS

Since the square of the Euclidean norm $\|\cdot\|^2$ is simply the sum of squares of each component, it follows that

$$\begin{aligned}\left\|\left|\mathbf{A}_W\mathbf{x}\right| - |\mathbf{m}|\right\|^2 &= \left\|\left|\begin{matrix}\mathbf{A}\mathbf{x}\\ \mu\mathbf{W}\mathbf{x}\end{matrix}\right| - \left|\begin{matrix}\mathbf{y}\\ \mathbf{0}\end{matrix}\right|\right\|^2 \\ &= \left\||\mathbf{A}\mathbf{x}| - |\mathbf{y}|\right\|^2 + \left\||\mu\mathbf{W}\mathbf{x}| - |\mathbf{0}|\right\|^2 \\ &= \left\||\mathbf{A}\mathbf{x}| - |\mathbf{y}|\right\|^2 + \mu^2\left\|\mathbf{W}\mathbf{x}\right\|^2\end{aligned}$$

where the last equality comes from the homogeneity property of norms. This formulation is close to a Tikhonov regularization problem, but the presence of the absolute values imposes for specific algorithms to be used.

ACKNOWLEDGMENTS

This work is supported in part by the European Union through the European Regional Development Fund (ERDF), and by the french region of Brittany, Ministry of Higher Education and Research, Rennes Métropole and Conseil Départemental 35, through the CPER Project SOPHIE/STIC & Ondes.

REFERENCES

[1] D. Löschenbrand and C. Mecklenbrauker, "Fast antenna characterization via a sparse spherical multipole expansion," in *4th International Workshop on Compressed Sensing Theory and its Applications to Radar, Sonar and Remote*, Aachen, 2016.

[2] R. Cornelius, D. Heberling, N. Koep, A. Behboodi, and R. Mathar, "Compressed sensing applied to spherical near-field to far-field transformation," in *Eur. Conf. Antennas Propag. (EuCAP)*, Davos, 2016.

[3] C. Culotta-López, D. Heberling, A. Bangun, A. Behboodi, and R. Mathar, "A compressed sampling for spherical near-field measurements," in *AMTA*, Williamsburg Virginia, USA, 2018.

[4] O. M. Bucci, C. Gennarelli, and C. Savarese, "Representation of electromagnetic fields over arbitrary surfaces by a finite and nonredundant number of samples," *IEEE Trans. on Antennas and Propag.*, vol. 46, no. 3, pp. 351–359, 1998.

[5] B. Fuchs and A. Polimeridis, "Reduced-order models for fast antenna characterization," *IEEE Trans. on Antennas and Propag.*, vol. 67, no. 8, pp. 5673–5677, 2019.

[6] N. Mézières, M. Mattes, and B. Fuchs, "Antenna characterization from a small number of far-field measurements via reduced-order models," *IEEE Trans. on Antennas and Propag.*, vol. 70, no. 4, pp. 2422–2430, 2022.

[7] G. Giordanengo, M. Righero, F. Vipiana, M. Sabbadini, and G. Vecchi, "Fast antenna testing with reduced near field sampling," *IEEE Trans. on Antennas and Propag.*, vol. 62, no. 5, pp. 2501–2513, 2014.

[8] O. Breinbjerg and J. Fernandez Álvarez, "Phaseless near-field antenna measurement techniques – an overview," in *AMTA*, United States, 2016.

[9] J. Hald, J. Hansen, F. Jensen, and F. Larsen, *Spherical Near Field Antenna Measurements*. Peter Peregrinus, 1988.

[10] R. Pierri and R. Moretta, "On data increasing in phase retrieval via quadratic inversion: Flattening manifold and local minima," *IEEE Trans. on Antennas and Propag.*, vol. 68, no. 12, pp. 8104–8113, 2020.

[11] F. Rodríguez Varela, J. Fernandez Álvarez, B. Galocha Iragüen, M. Sierra Castañer, and O. Breinbjerg, "Numerical and experimental investigation of phaseless spherical near-field antenna measurements," *IEEE Trans. on Antennas and Propag.*, vol. 69, no. 12, pp. 8830–8841, 2021.

[12] O. Bucci, G. D'Elia, G. Leone, and R. Pierri, "Far-field pattern determination from the near-field amplitude on two surfaces," *IEEE Trans. on Antennas and Propag.*, vol. 38, no. 11, pp. 1772–1779, 1990.

[13] T. Isernia, G. Leone, and R. Pierri, "Radiation pattern evaluation from near-field intensities on planes," *IEEE Trans. on Antennas and Prop.*, vol. 44, no. 5, pp. 701–, 1996.

[14] R. Yaccarino and Y. Rahmat-Samii, "Phaseless bi-polar planar near-field measurements and diagnostics of array antennas," *IEEE Trans. on Antennas and Propag.*, vol. 47, no. 3, pp. 574–583, 1999.

[15] F. Las-Heras and T. Sarkar, "A direct optimization approach for source reconstruction and nf-ff transformation using amplitude-only data," *IEEE Trans. on Antennas and Prop.*, vol. 50, no. 4, pp. 500–510, 2002.

[16] B. Fuchs, M. Mattes, S. Rondineau, and L. Le Coq, "Phaseless near-field antenna measurements from two surface scans — numerical and experimental investigations," *IEEE Trans. on Antennas and Propag.*, vol. 68, no. 3, pp. 2315–2322, 2020.

[17] S. Costanzo, G. Di Massa, and M. Migliore, "A novel hybrid approach for far-field characterization from near-field amplitude-only measurements on arbitrary scanning surfaces," *IEEE Trans. on Antennas and Propag.*, vol. 53, no. 6, pp. 1866–1874, 2005.

[18] F. Rodríguez Varela, B. Iragüen Galocha, and M. Castañer Sierra, "Practical considerations in phaseless spherical near-field measurements," in *AMTA*, 2021.

[19] E. J. Candès, X. Li, and M. Soltanolkotabi, "Phase retrieval via wirtinger flow: Theory and algorithms," *IEEE Transactions on Information Theory*, vol. 61, no. 4, pp. 1985–2007, 2015.

[20] A. Bangun, A. Behboodi, and R. Mathar, "Signal recovery from phaseless measurements of spherical harmonics expansion," in *2019 27th European Signal Processing Conference (EUSIPCO)*, 2019.

[21] E. J. Candès, T. Strohmer, and V. Voroninski, "Phaselift: Exact and stable signal recovery from magnitude measurements via convex programming," *Communications on Pure and Applied Mathematics*, vol. 66, no. 8, pp. 1241–1274, 2013. [Online]. Available: https://onlinelibrary.wiley.com/doi/abs/10.1002/cpa.21432

[22] A. Bangun, C. Culotta-López, A. Behboodi, R. Mathar, and D. Heberling, "On phaseless spherical near-field antenna measurements," in *2019 13th European Conference on Antennas and Propagation (EuCAP)*, 2019, pp. 1–5.

[23] A. Guth, C. Culotta-López, J. Maly, H. Rauhut, and D. Heberling, "Polyhedral sampling structures for phaseless spherical near-field antenna measurements," in *AMTA*, 2020.

[24] J. Wang, Y. Wen, and D. Zhang, "Phaseless bi-spherical near-field measurement," in *2022 International Conference on Electromagnetics in Advanced Applications (ICEAA)*, 2022, pp. 009–014.

[25] J. Wang, Y. Wen, D. Zhang, and J. Zhang, "Phaseless spherical near-field to far-field transformation algorithm via sparsity of spherical mode coefficients," *International Journal of Antennas and Propagation*, 2022.

[26] A. Paulus, J. Knapp, and T. F. Eibert, "Phaseless near-field far-field transformation utilizing combinations of probe signals," *IEEE Trans. on Antennas and Propag.*, vol. 65, no. 10, pp. 5492–5502, 2017.

[27] C. Schmidt, S. Razavi, T. Eibert, and Y. Rahmat-Samii, "Phaseless spherical near-field antenna measurements for low and medium gain antennas," *Advances in Radio Science*, vol. 8, pp. 43–48, 2010.

[28] N. Mézières and L. Le Coq, "Improvement of the gerchberg-saxton algorithm convergence in phaseless antenna measurements via spherical wave filtering," *early access in IEEE Transactions on Antennas and Propagation*, 2023.

[29] N. Mézières, L. Le Coq, and B. Fuchs, "Antenna far-field characterization from small phaseless dataset," in *AMTA*, Denver, 2022.

[30] R. Chandra, Z. Zhong, J. Hontz, V. McCulloch, C. Studer, and T. Goldstein, "Phasepack: A phase retrieval library," 2017.

[31] B. Fuchs, L. Le Coq, S. Rondineau, and M. Migliore, "Fast antenna far field characterization via sparse spherical harmonic expansion," *IEEE Trans. on Antennas and Propag.*, vol. 65, no. 10, pp. 5503–5510, 2017.

[32] "CST studio suite 2020," Dassault Systèmes, 2020, available at https://www.3ds.com/fr/produits-et-services/simulia/produits/cst-studio-suite/.

[33] P. Hansen, "The L-curve and its use in the numerical treatment of inverse problems," in *Computational Inverse Problems in Electrocardiology*. WIT Press, 2000.

[34] N. Mézières, B. Fuchs, L. Le Coq, J.-M. Lerat, R. Contreres, and G. Le Fur, "On the application of sparse spherical harmonic expansion for fast antenna far field measurements," *IEEE Antennas and Wireless Propagation Letters*, 2020.

[35] "Starlab 650MHz-18GHz," MVG, 2020, available at https://www.mvg-world.com/fr/products/antenna-measurement/multi-probe-systems/starlab.